Peer-reviewed version available at ChemEngineering 2018, 2, 32; doi:10.3390/chemengineering2030032

Article

Experimental Study and Hydrodynamic Modelling of the Wet Agglomeration Process

Benjamin Oyegbile [1,*], Guven Akdogan [1] and Mohsen Karimi [2]

[1] Department of Process Engineering, Stellenbosch University, Banghoek & Bosman Road, Stellenbosch 7600 South Africa; gakdogan@sun.ac.za
[2] Department of Chemistry and Chemical Engineering, Chalmers University of Technology, 41296 Gothenburg, Sweden; mohsenk@chalmers.se
* Correspondence: oyegbile@sun.ac.za; Tel.: +27-(0)21-808-9485

Abstract: In this study, an experimentally validated computational model was developed to investigate the hydrodynamics in a rotor-stator vortex RVR agglomeration reactor having a rotating disc at the centre with two shrouded outer plates. A numerical simulation was performed using a simplified form of the reactor geometry to compute the 3D flow field in batch mode operations. Thereafter, the model was validated using data from a 2D Particle Image Velocimetry (PIV) flow analysis performed during the design of the reactor. Using different operating speeds—70, 90, 110 and 130 rpm, the flow fields were computed numerically followed by a comprehensive data analysis. The simulation results showed separated boundary layers on the rotating disc and the stator. The flow field within the reactor is characterized by a rotational plane circular forced vortex flow in which the streamlines are concentric circles with a rotational vortex. Overall, the results of the numerical simulation demonstrate a fairly good agreement between the CFD model and the experimental data as well as the available theoretical predictions. The swirl ratio β was found to be approximately 0.4044, 0.4038, 0.4044 and 0.4043 for operating speeds of N=70, 90, 110 and 130 rpm respectively. In terms of the spatial distribution, the turbulence intensity and kinetic energy are concentrated on the outer region of the reactor while the axial velocity showed a decreasing intensity towards the shroud. However, a comparison of the CFD and experimental predictions of the tangential velocity and the vorticity amplitude profiles shows that these parameters were under-predicted by the experimental analysis which could be attributed to some of the experimental limitations rather than the robustness of the CFD model or numerical code.

Keywords: wet agglomeration; flocculation; hydrodynamics; turbulence

1. Introduction

The removal of particulate solids from liquid process effluent is of great importance in environmental quality management. However, when the sizes of solid particles diminish and reach micron and submicron range, the particles tend to remain in suspension and cannot be removed by gravity settling [1,2]. In order to achieve an acceptable solid-liquid separation at a reasonable cost, the particles need to be agglomerated by flocculation followed by mechanical phase separation—sedimentation, floatation, filtration etc. The agglomeration of suspended particles to form larger and settleable flocs form the basis of operation of many process industries ranging from municipal water and wastewater treatment to pulp and paper processing.

Mixing plays an important role in the agglomeration of fine particles in suspension either in engineered or natural systems and the choice of a particular stirrer-vessel configuration strongly influences the flow pattern in the treatment unit. Flow in the wheelspace or cavity between a stationary and rotating disc (rotor-stator system) is of great importance in many engineering applications such as in mixing applications for food, chemical and pharmaceutical industries, and in the turbine and compressor blades for the aeronautical industry [3–6]. Flows of this nature has been the subject of many scientific investigations both theoretically and experimentally [7,8]. Theoretical

analysis of the nature of flow in rotor-stator systems resulted in the so called—Batchelor-Stewartson controversy regarding the exact nature of the flow profile in the wheelspace between the rotor and the stator. It is now generally accepted that both models are valid with the Batchelor's model giving more accurate description of the flow in an enclosed or shrouded rotor-stator system which consist of a separated boundary layers on the rotor and the stator and an inviscid rotating core in between the boundary layers [9,10].

The use of Computational Fluid Dynamics CFD for the investigation of complex fluid-particle interactions in many engineering design of fluid flow applications has been steadily growing in popularity, both in academia and the industry over the past few decades [11,12]. Nowadays, numerical simulations complement the experimental and analytical techniques, and are increasingly being performed on a much bigger scale in many fluid engineering applications ranging from chemical and mineral processing to civil and environmental process engineering [11]. In any design-based CFD modelling, the main focus is to assess the hydrodynamics of the system and to determine the flow pattern, hydrodynamic profile—velocity, vorticity, kinetic energy, dissipation rates, turbulence intensity, turbulent viscosity profiles etc., dead zones and black spots which in turn, will help in improving and optimizing the engineering design and overall performance of the reactor [13,14]. In many technical applications of engineering design techniques to complex fluid flow problems, an understanding of the interacting physical, biological and chemical processes within the reactor system is highly indispensable. This is particularly interesting as the CFD offers a flexible and sophisticated platform for engineers and scientists in the investigation of complex engineering design problems. A quick survey of literature in this field shows that many innovative fluid-particle multiphase reactors have been successfully designed and tested on different scales for a wide range of engineering applications ranging from particle separation and water purification—bacterial inactivation, to biological cell culture preparation [15–22]. For instance, the application of Taylor-vortex or Taylor-Couette flow for a wide range of beneficial physicochemical treatments have been reported with some encouraging results [23].

Buwa et al. [3,4] investigated the performance and optimization of different types of disc impellers as flow inducers in stirred tanks. Their two-part study compared the efficiency of the rotating disc to the conventional propeller as alternative flow inducers in mixing tank applications. A radial grid disc, square grid disc, solid discs and a propeller were selected for the investigation. Laser Doppler Anemometry—LDA measurements and the subsequent numerical simulation showed that there was no substantial variation in the axial flow pattern between the radial grid and the square grid disc. However, the flow near the impeller shows a strong dependence on the impeller configuration. The study also reported that the mixing performance of the radial grid disc and that of the propeller was roughly the same. Similarly, Dionysios et al. [19] investigated the application of rotating disc photocatalytic reactor—RDPR for the treatment of organic pollutants in water. A subsequent analysis of the mixing and treatment efficiency in terms of the degradation of the organic pollutants showed that the technique offers several benefits when compared to the existing ones and the mixing regime is quite close to that of the continuous stirred tank reactor CSTR. However, vital information on the hydrodynamic behaviour of the reactor either experimentally or numerically was missing from the study. In the case of technical applications of Batchelor vortex, it is the comprehensive study of a multi-inlet vortex reactor by Liu et al. [24,25] that has advanced research in this field to the greatest extent. Their two-part study reported that the flow structure of the vortex flow in the nano particle precipitation reactor consist of a spiral motion in the free-vortex region and a nearly homogeneous mixing in the forced-vortex region.

While there appears to be huge interest in rotor-stator flow among the scientific community from theoretical perspective, it is very rare to find practical applications of this type of flow especially in fluid-particle separation with the exception of Taylor-Couette flow. Therefore, the aim of this study is to investigate the hydrodynamic performance of a rotor-stator vortex agglomeration reactor—RVR designed for fluid-particle separation using Batchelor flow in a shrouded cavity. A single rotating reference frame SRF approach was used to model the disc interaction with the fluid domain coupled with k-ε and RSM turbulence closure models. The validated CFD model is

subsequently employed in analysing the flow pattern and the spatial distribution of the hydrodynamic quantities within the reactor and in understanding the hydrodynamic behaviour with respect to the reactor geometry.

2. Materials and Methods

2.1 Description of the RVR Agglomeration Reactor

A patented rotating disc vortex reactor RVR made from perspex was designed for the agglomeration of dispersed fine particles in suspension as shown schematically in **Fig.1a** with the design details available elsewhere [26]. It is of cylindrical rotor-stator configuration with a shrouded outer casing. The working slurry is a mixed synthetic kaolin suspension fed into the reactor through an opening at the top. Mixing of the synthetic suspension—kaolin slurry and the flocculating agents (synthetic poly acrylamide PAM—Superfloc® C-492 and N-300) is provided by the spinning disc powered by a rotating shaft. The rotating disc made from PVC generates both radial swirling flow at the immediate vicinity of the disc and an axially pumping flow at some distance away from the disc towards the stator, which eventually drives the agglomerated flocs towards the shroud of the reactor as shown schematically in **Fig. 1b**. The axial flow away from the rotating disc towards the shroud facilitates the collection of densified agglomerates on either side of the reactor in batch mode operations.

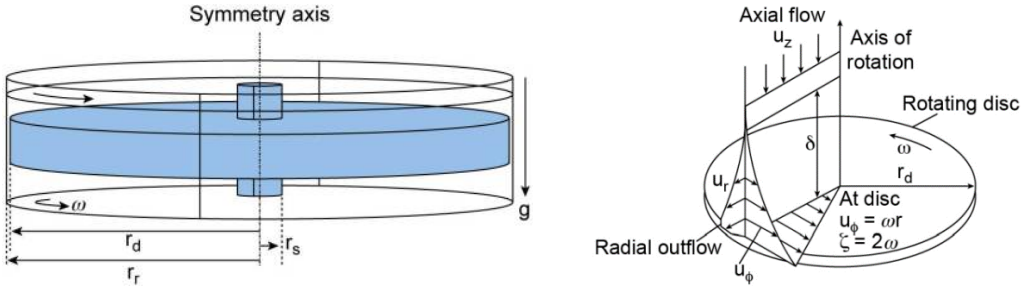

(a) (b)

Fig. 1: Schematic illustration of the reactor configuration and flow profiles (a) RVR reactor (b) rotor-stator flow boundary layers showing the tangential velocity and vorticity amplitude profiles on the rotating disc (Reproduced from [8] with permissions © 2011 Elsevier).

2.2 Theoretical Analysis of the Fluid Flow

The flow in the reactor wheelspace or cavity is characterized by an axis-symmetrical forced vortex Batchelor flow with separated boundary layers at the rotor and the stator. The velocity profile of the flow on the disc boundary layer is illustrated in **Fig. 1b** with radial, tangential and axial velocity flow profiles. The circumferential velocity in a forced vortex flow increases radially outwards with the radius attaining a maximum at the tip of the disc—tip velocity, while the vorticity magnitude is nearly constant with its amplitude twice the angular velocity of the rotating disc. The flow in the reactor system—either on the boundary layer or rotating core may be characterized by a certain degree of flow instability when it is above the critical Reynolds number $Re_{\varphi,\,critical} \approx 2 \times 10^5$ with small patches of turbulence or oscillating vortex disturbance [7,8]. This can be expressed mathematically for the boundary layer near the rotor using the local rotational Reynolds number $Re_{\varphi,\,local}$ (**Eq. 1**). The gap ratio G of the reactor defined as the ratio of the wheelspace width to the outer disc radius is approximately 0.2206 for this reactor system (**Eq. 2**). The theoretical hydrodynamic characteristic values are given in **Table 1**.

Peer-reviewed version available at ChemEngineering 2018, 2, 32; doi:10.3390/chemengineering2030032

Table 1: Theoretical values of the flow quantities at different operating speeds near the rotating disc boundary layer

	Hydrodynamic parameters		
Operating speeds (rpm)	Disc rotational Reynolds number (-)	Disc tip velocity (ms-1)	Disc vorticity (s-1)
70	2.59 × 104	0.4985	14.662
90	3.33 × 104	0.6410	18.852
110	4.07 × 104	0.7834	23.041
130	4.81 × 104	0.9258	27.231

$$Re_{\phi,\,local} = \left(\frac{r}{r_d^2}\right)\frac{\rho\omega r^2}{\mu} = \frac{\rho\omega r^2}{\mu} \quad (1)$$

$$G = \frac{s}{r} \quad (2)$$

2.3 Experimental Fluid Flow Measurements

The flow measurement commences after running the reactor for a period of time in which the fluid flow had reached a steady state. In our case, we assume a time longer than $t = tG_{\varphi} = 25s$ as the time at which the system has reached a pseudo-steady state condition [27]. The 2D PIV measurements which is described in details elsewhere [15] consist of a RVR reactor system seeded with tracing particles and distilled water at standard conditions as working fluid (**Fig. 2**). The geometry of the reactor presented some measurement constraints which was taken into account in the post-processing and analysis of the experimental data. The laser system for the experimental measurements consist of a LINOS Nano 259-532-100 (Qioptic GmbH & Co. KG, Germany) providing illumination for a cross section of the reactor under investigation. A high resolution CMOS camera was used to capture the steady state fluid flow behaviour for post-processing and cross-correlation in MATLAB (Mathworks GmbH, Germany). The seeding particles is a mixture (1:1) of silver-coated and hollow glass spheres (Dantec Dynamics, A/S, Denmark) measuring 10μm in average diameter with good light scattering efficiency and sufficiently small velocity lag [28,29].

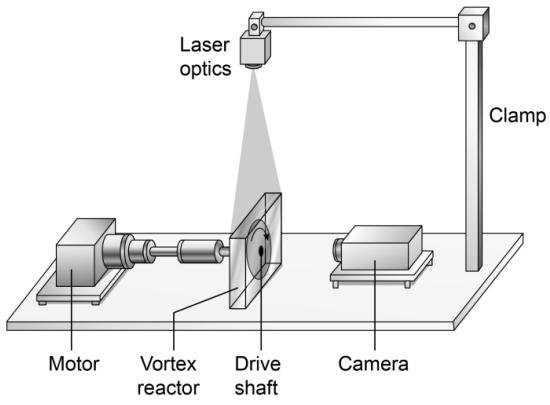

Fig. 2: Schematic illustration of the particle Image Velocimetry (PIV) set up.

Preprints (www.preprints.org) | NOT PEER-REVIEWED | Posted: 29 May 2018 doi:10.20944/preprints201805.0420.v1

Peer-reviewed version available at ChemEngineering 2018, 2, 32; doi:10.3390/chemengineering2030032

3. Numerical Simulation

3.1 Model Description

3.1.1 Governing Equations

The general form of the governing equations of mass and momentum conservation or the so called—Reynolds-Averaged Navier-Stokes (RANS) equation can be written in a simplified form for a steady-state single phase fluid flow is given in **Eqs. 3-4**, where ρ is the density, p is the static pressure, $\vec{v}$ is the velocity component, $\bar{\bar{\tau}}$ represents the stress tensor due to viscous stress, $\rho\vec{g}$ is the gravitational force and $\vec{F}$ is the exerted body forces. The Reynolds Averaged (RANS) form of the continuity and momentum conservation equations was used along with k-ε eddy-viscosity and RSM turbulence models to close the RANS momentum equation. In the case of standard and RNG k-ε models, this is done by calculating the turbulent or eddy viscosity μ_t, or effective viscosity μ_{eff} from the transport equations of turbulent kinetic energy k and its dissipation rate ε [4,30,31]. The effective viscosity μ_{eff} and the stress tensor $\bar{\bar{\tau}}$ can be written as follows where μ represent the molecular viscosity and the constant C_μ=0.09, and 0.0845 for the standard k-ε and RNG k-ε models respectively, while the last terms on the right represent the turbulent or eddy viscosity (**Eqs. 5-6**) [4,32–35]:

$$\frac{\partial \rho}{\partial t} + \nabla\cdot(\rho\vec{v}) = 0 \tag{3}$$

$$\frac{\partial}{\partial t}(\rho\vec{v}) + \nabla\cdot(\rho\vec{v}\vec{v}) = -\nabla p + \nabla\cdot(\bar{\bar{\tau}}) + \rho\vec{g} + \vec{F} \tag{4}$$

$$\mu_{eff} = \mu + \frac{\rho C_\mu k^2}{\varepsilon} \tag{5}$$

$$\bar{\bar{\tau}} = \mu\left[(\nabla\vec{v} + (\nabla\vec{v})^T\right] - \frac{2}{3}\mu\delta\nabla\vec{v} \tag{6}$$

3.1.2 Fluid Flow Domain, Mesh and Grid Convergence

A solid modelling software (ANSYS DesignModeler 18.2, ANSYS Inc.) was used to create the simplified CAD model of the reactor along with the rotating disc to describe the fluid domain (**Fig. 3**). Thereafter, a computational mesh was generated from the solid model for the computational study which consist of structured hexahedral mesh using the commercial grid generation software ANSYS Meshing 18.2 (ANSYS Inc.). Four grids of different mesh densities of approximately (0.042×10^6, 0.431×10^6, 0.86×10^6, and 1.3×10^6 elements) were created for the grid independence study. The grid independence study was conducted by carrying out the numerical simulation on successively finer grids. Thereafter, the results of the circumferential velocities were compared for all the grids to establish that they are grid-independent. Finally, a mesh containing approximately half a million elements was thereafter chosen on the basis of a trade-off between the required computational accuracy and CPU time needed to run the simulation to a converged solution. This optimized mesh was then used for subsequent computations of all parameters of interest with a computation time of

Preprints (www.preprints.org) | NOT PEER-REVIEWED | Posted: 29 May 2018 doi:10.20944/preprints201805.0420.v1

Peer-reviewed version available at ChemEngineering 2018, 2, 32; doi:10.3390/chemengineering2030032

approximately 15 hours for the highest operating speed. **Fig. 4** shows the radial and axial circumferential velocity profiles along Y-Z and X-Z planes at x=0.003725 and y=0.045 respectively for a rotation speed of 70rpm for all the four grids employed for the grid convergence study and clearly demonstrates that the results are grid-independent.

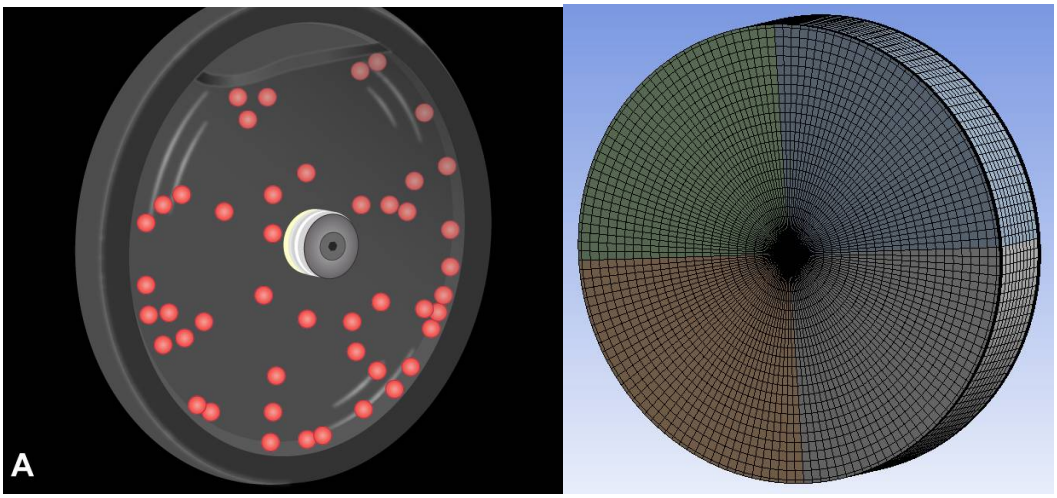

Fig. 3: Graphical illustration of the simplified reactor solid model and the generated computational grid for the numerical simulation.

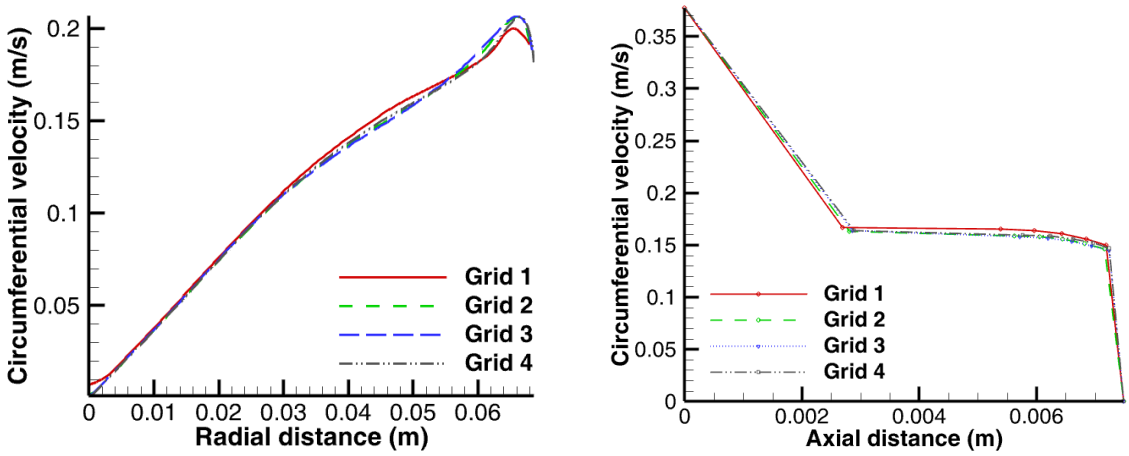

Fig. 4: Influence of the computational grid size on the computed radial and axial circumferential velocity profiles along Y-Z plane and X-Z plane parallel to the shaft for RNG k-ε model at 70 rpm (a) x=0.003725 (b) y=0.045.

3.2 Numerical Methods and Boundary Conditions

The hydrodynamics of the wet agglomeration process was investigated by obtaining numerically, the steady state flow field of a single phase flow in the reactor. This flow field was then compared to the experimentally derived one based on the assumption that the seeding particles in the PIV measurement faithfully follow the flow and do not have any impact on the continuous phase—one way coupling. This assumption is necessary to match the PIV experimental conditions. However, this simplified approach is rarely the case in practice. The agglomeration, growth and breakage of particle clusters—flocs ultimately lead to an exchange of momentum and energy

between the carrier and the particulate phase through contacts and collisions, especially for high particle concentration or dense flows [36,37]. In modelling the single phase flow in the agglomeration reactor, the Single Reference Frame SRF approach was employed with relative velocity formulation. This is due to the fact that most of the flow in the fluid domain is rotating as the flow inducer is in close proximity to the reactor wall. No slip condition was imposed on all walls with the choice of a relative reference frame to describe the zones relative to one another. The pressure-based coupled algorithms was used to obtain a steady state numerical solution of the Navier-Stokes Equation. This algorithm has been shown to offer a more robust and efficient single phase implementation for steady-state flows [33].

In order to ensure the accuracy of the numerical solution, the scaled residuals, moment on the revolving plate about the axis of rotation, and the average turbulent kinetic energy k were monitored until these parameters reduce to minimal or constant values and this forms the basis for assessing the convergence of the solution. In verifying the accuracy of the numerical solution, the theoretical values of some hydrodynamic quantities such as the tip velocity Ω of the rotating disc, the induced vorticity ζ on the disc boundary layer, the flow swirl ratio β and the gap ratio G were also calculated and compared to the numerically derived and literature values (**Fig. 1b**, **Eqs. 7-9**). Finally, validation of the numerical results was carried out by comparing some of the CFD results with the PIV data and the Batchelor model.

$$\Omega = \omega r = 2\pi n r \tag{7}$$

$$\zeta = 2\omega \tag{8}$$

$$\beta = \frac{\omega'}{\Omega} \tag{9}$$

4. Results and Discussion

The results of the CFD analysis showing the distribution of the mean flow parameters is hereby presented in the following sections. Only the data from one side of the reactor is analysed as the flow is fully symmetrical about the axis of rotation. The symmetrical nature of the flow was also confirmed in the course of the data analysis by comparing data points on either side of the reactor and other points of symmetry. It can be clearly seen that the flow fields are generally similar in structure but mainly differ in terms of the flow quantities' magnitude.

4.1. Analysis of the Mean Flow Characteristics

4.1.1 Radial Distribution of the Hydrodynamic Quantities

The flow streamlines in the rotor-stator system can be analysed on the basis of the Batchelor flow model. The flow structure in the RVR reactor broadly agrees with the Batchelor's predictions and that of several other similar studies [9,10]. The Batchelor's prediction was arrived at by solving a simplified form of Navier-Stokes equation to obtain an approximate flow field. **Figs. 5a-d and 6a-d** shows the radial profiles of the circumferential velocity vector fields and contours and the vorticity vector maps and contours on the rotating disc boundary layer and on three Y-Z planes along the

Preprints (www.preprints.org) | NOT PEER-REVIEWED | Posted: 29 May 2018 doi:10.20944/preprints201805.0420.v1

Peer-reviewed version available at ChemEngineering 2018, 2, 32; doi:10.3390/chemengineering2030032

reactor wheelspace which seems to be consistent with the theoretical descriptions given in **Fig. 1b** and **Eqs. 6 and 7**. Away from the boundary layer near the rotor, there is a sharp increase the radial vorticity profile with respect to the radial distance (**Figs. 6b-d**). In addition, the radial circumferential velocity profile shows a somewhat lower magnitude than the tip velocity close to the wall of the reactor (**Fig. 4a**). However, in the case of the vorticity magnitude profile, it is observed that there is a small region of high vorticity mostly around the outer edge of the rotating disc as shown in the vorticity magnitude contour (**Fig. 5a**). Apart from this region, the CFD results is consistent with the theoretical prediction of vorticity as twice the magnitude of the rotating disc angular velocity (**Fig. 1b, Table 1**). It has been shown by previous studies that a region of high vortex and vorticity tend to promote the wet agglomeration of particles and floc densification [38,39]. However, owing to the nature of the clearance between the rotating disc and the reactor wall, which is quite narrow, it is not possible to take advantage of this rotational effect for further densification of the formed flocs and this will be a factor to be considered in future optimization of the reactor system. The velocity distribution across the wheelspace is characterized by Batchelor flow with separated boundary layers and an inviscid core that rotates at a fraction of the rotor angular velocity with an axial pumping effect towards the shroud. The swirl ratio β which is a measure of the ratio of the rotating core tangential velocity to that of the disc tip velocity or boundary layer velocity was found to be approximately 0.4044, 0.4038, 0.4044 and 0.4043 for operating speeds of N=70, 90, 110 and 130 rpm respectively which are quite similar to the values reported by Daily et al. [8].

The basic outline of the flow pattern is also consistent with the PIV results which are available elsewhere [15]. The velocity profiles at two selected YZ cross sections on the model were validated by comparing them with the experimental data with a measurement error of ± 0.05. (**Figs. 5b and 5c**). In general, the velocity profile shows a fairly good agreement with the PIV data except at the outer edge of the cross section of the PIV velocity profile. This region on the outer edge of the cross section had to me masked out in the post-processing of the PIV data owing to some measurement limitations encountered during the PIV analysis. The high fluctuation of the laser signal on the fluid surface makes the measurement quite a challenge. Compared with the PIV results, the maximum tangential velocity predicted by the CFD differs by a value of approximately 10%. However, it is worth pointing out that the observed deviations of the CFD data from the experimental results were mainly due to the experimental limitations encountered in the PIV analysis rather than the accuracy of the numerical predictions. A quick comparison of the CFD data with theoretical calculations in **Table 1** seems to suggest that the PIV analysis under predicted the flow characteristics.

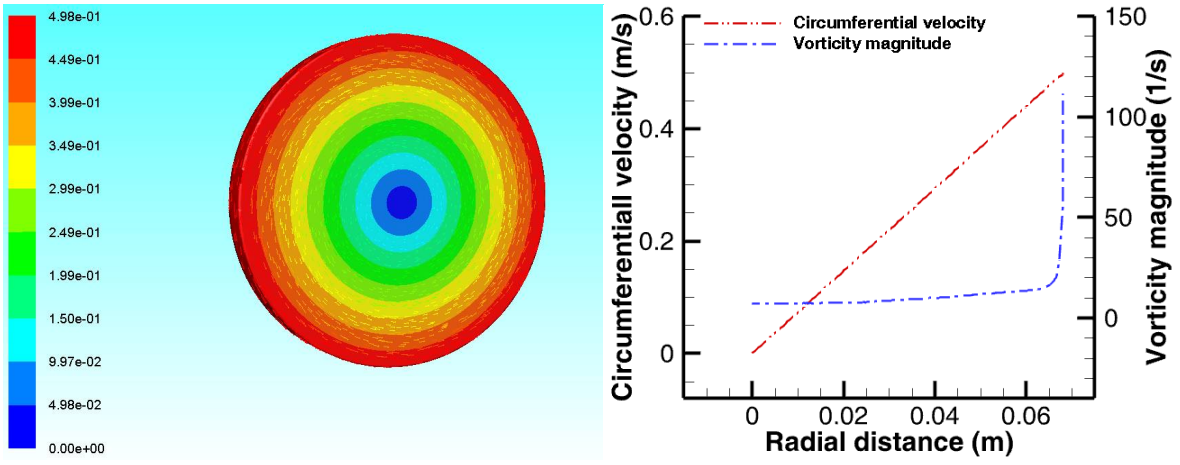

(a)

Preprints (www.preprints.org) | NOT PEER-REVIEWED | Posted: 29 May 2018 doi:10.20944/preprints201805.0420.v1

Peer-reviewed version available at ChemEngineering 2018, 2, 32; doi:10.3390/chemengineering2030032

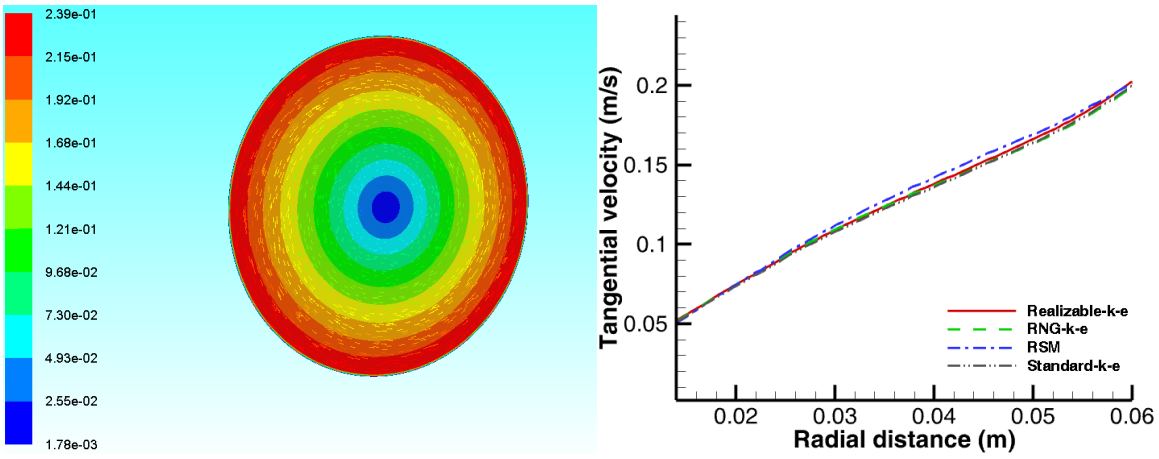

(b)

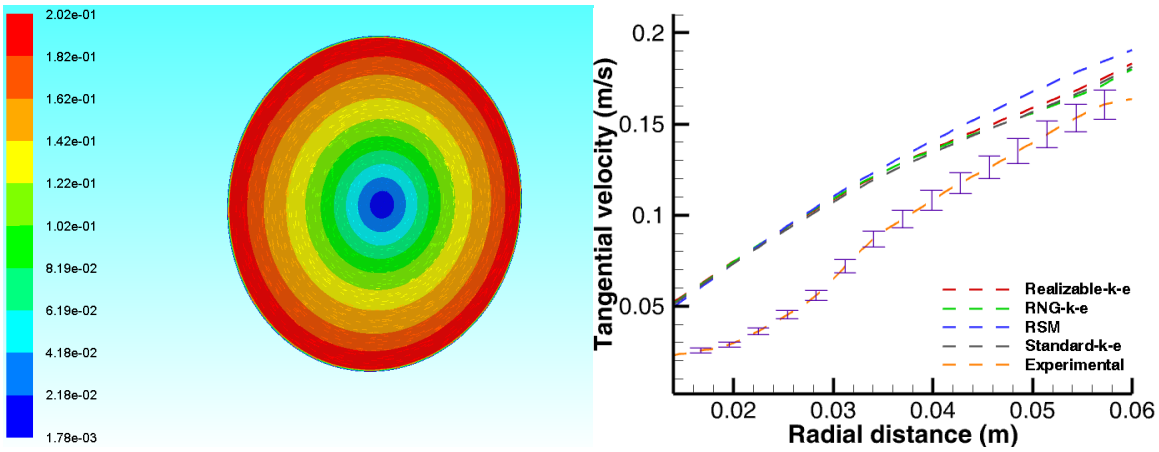

(c)

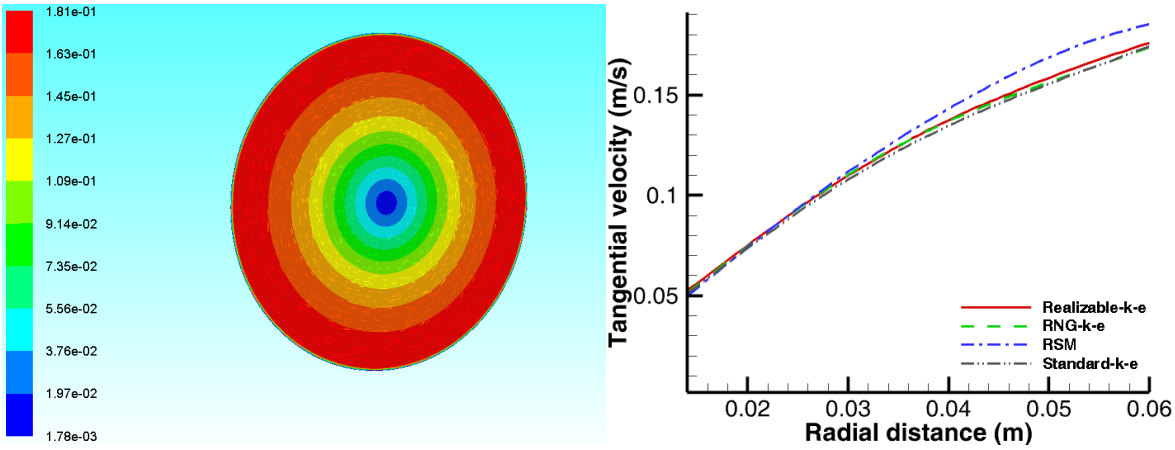

(d)

Fig. 5: Reactor cross sections showing the velocity vector fields and contours for RNG-k-ε model for and radial tangential velocity profiles along Y-Z plane at *N*=70rpm (a) rotating disc boundary layer (b) x=0.0015 (c) x=0.003725 (d) x=0.006.

Peer-reviewed version available at ChemEngineering 2018, 2, 32; doi:10.3390/chemengineering2030032

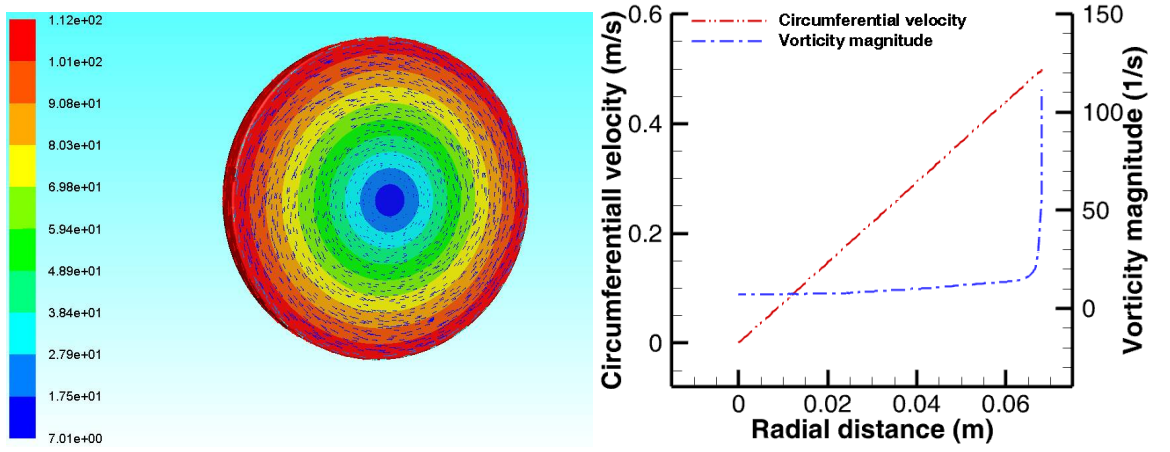

(a)

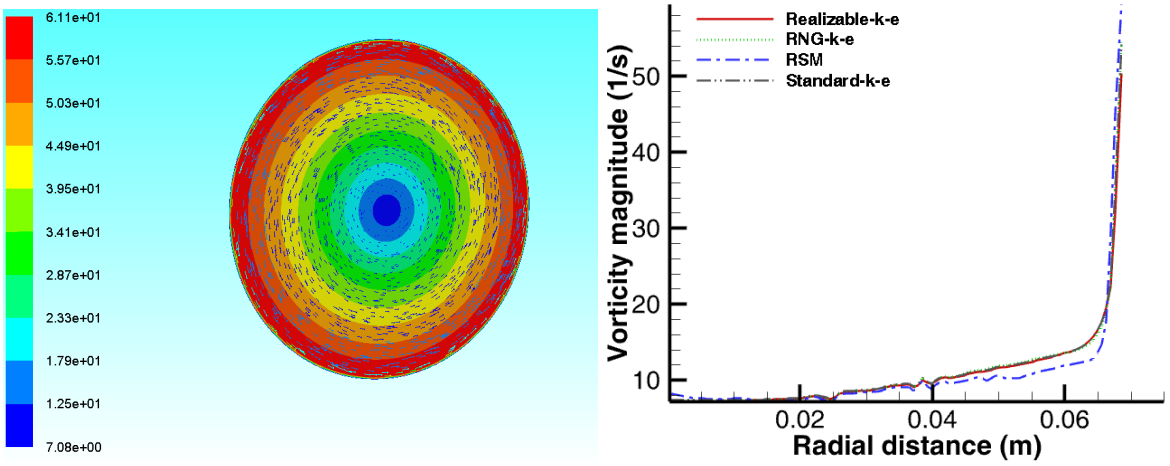

b)

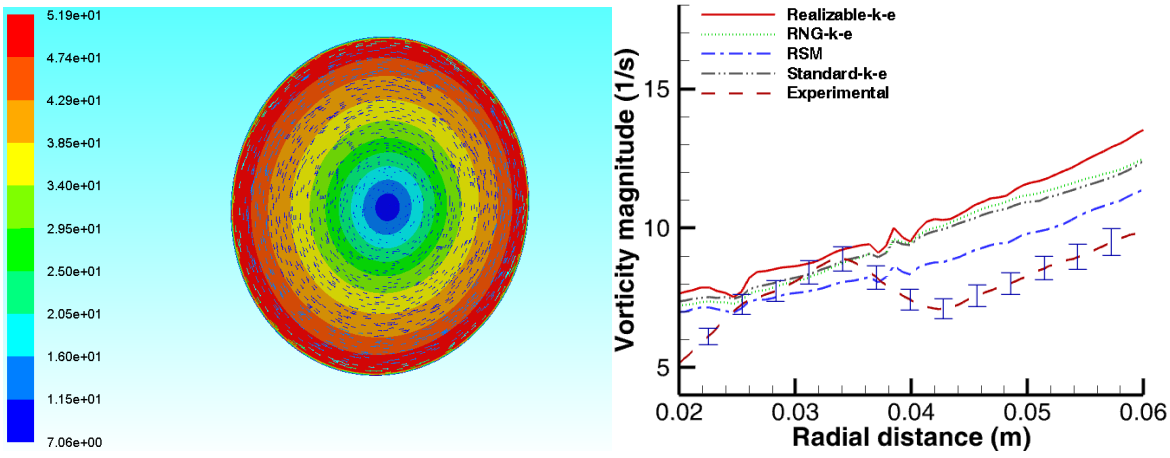

(c)

Preprints (www.preprints.org) | NOT PEER-REVIEWED | Posted: 29 May 2018 doi:10.20944/preprints201805.0420.v1

Peer-reviewed version available at ChemEngineering 2018, 2, 32; doi:10.3390/chemengineering2030032

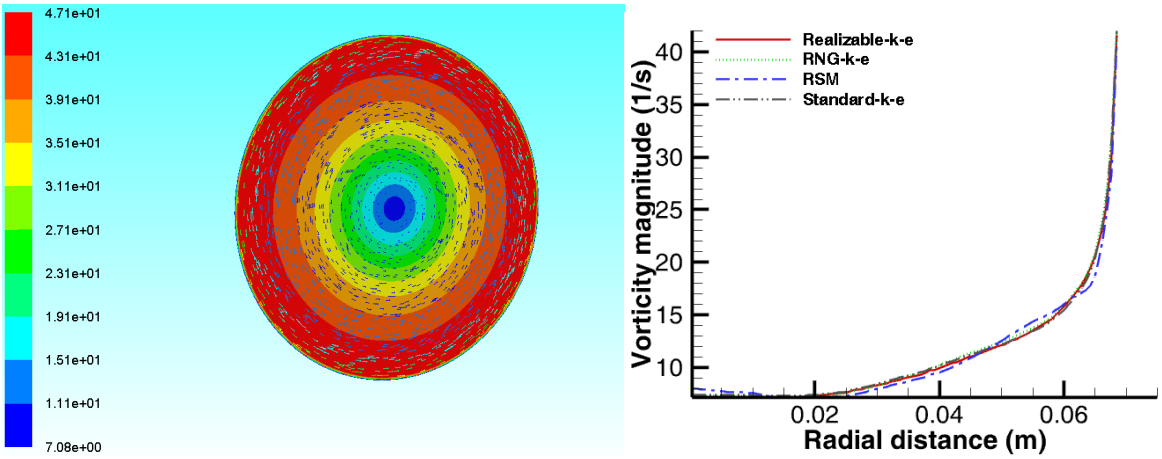

(d)

Fig. 6: Reactor cross sections showing the vorticity vector maps and contours RNG-k-ε model and radial vorticity magnitude profiles along Y-Z plane at *N*=70rpm (a) rotating disc boundary layer (b) x=0.0015, (c) x=0.003725 (d) x=0.006.

4.1.2 Axial Distribution of the Hydrodynamic Quantities

The tangential velocity U_ϕ contours and profiles and the vorticity amplitude ζ contours and profiles on the XZ plane are shown in **Figs. 7a-c and 8a-c** respectively. The axial tangential velocity distribution shows a pattern consistent with Batchelor flow profile except on plane y=0 near the shaft where the velocity is zero as expected. **Figs. 7a-c** show a varying pattern of Batchelor velocity profiles but with distinct separated boundary layers and a central rotating core. By contrast, the width of the rotor boundary layer is slightly longer and the rotating core slightly shorter when compared to the Batchelor profile (**Fig. 11b**). In terms of the axial vorticity amplitude, all the profiles seem to be identical as except on plane y=0 at the region close to the shaft where the vorticity amplitude remains constant throughout the plane (**Fig. 8a**). Overall, the velocity and the vorticity amplitude increases with the axial plane height with plane y=45 recording the highest magnitude. However, there is a region of high vorticity mostly on the outer edge of the rotating disc close to the reactor wall. This observation is quite interesting as it suggests that the clearance between the disc and the reactor wall might strongly influence the vorticity magnitude. The influence of the gap ratio *G* on the fluid flow cannot be ruled out and a detailed geometry parametric investigation prior to the scale-up of the reactor in future can yield some useful data for design optimization.

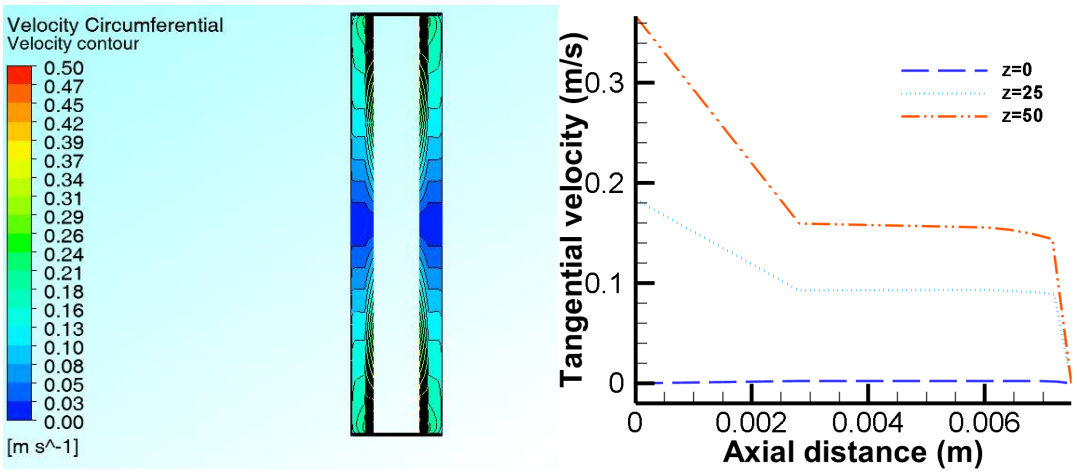

(a)

Preprints (www.preprints.org) | NOT PEER-REVIEWED | Posted: 29 May 2018 doi:10.20944/preprints201805.0420.v1

Peer-reviewed version available at ChemEngineering 2018, 2, 32; doi:10.3390/chemengineering2030032

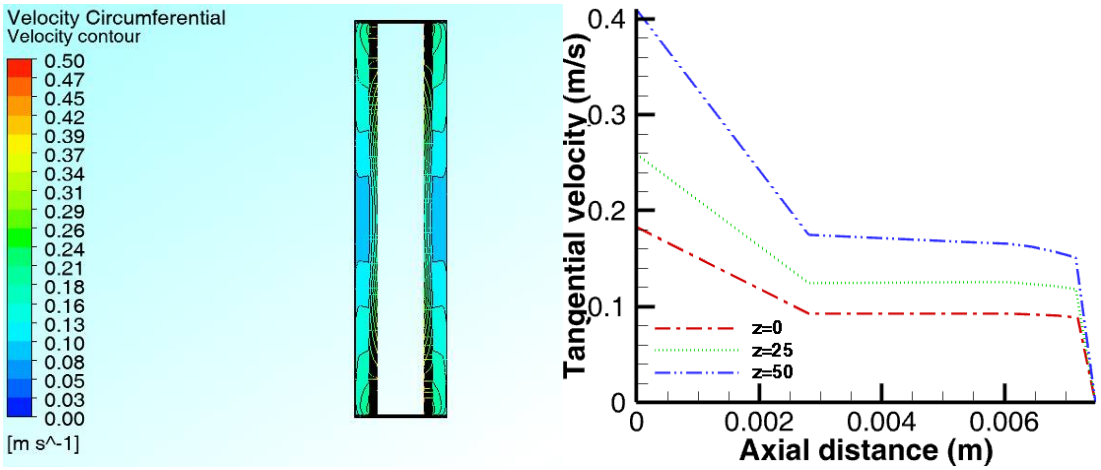

(b)

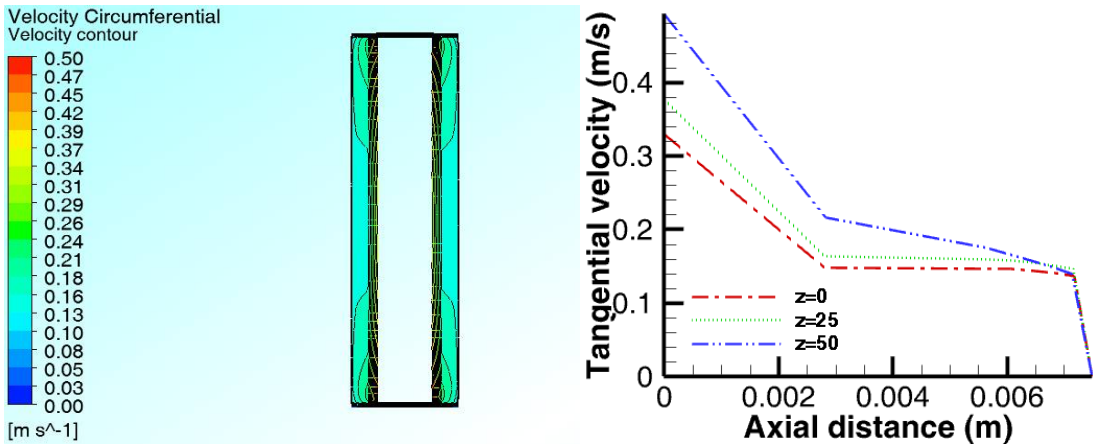

(c)

Fig. 7: Reactor cross sections showing the velocity contours and axial tangential velocity profiles along three horizontal lines on X-Z plane at *N*=70rpm—RNG model (a) y=0, (b) y=0.025 (c) y=0.045.

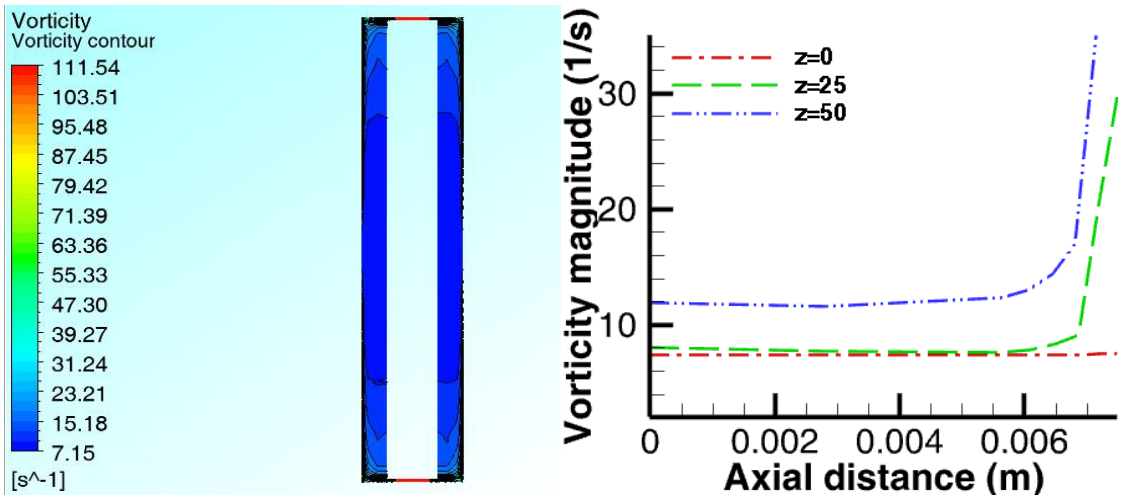

(a)

Preprints (www.preprints.org) | NOT PEER-REVIEWED | Posted: 29 May 2018 doi:10.20944/preprints201805.0420.v1

Peer-reviewed version available at ChemEngineering 2018, 2, 32; doi:10.3390/chemengineering2030032

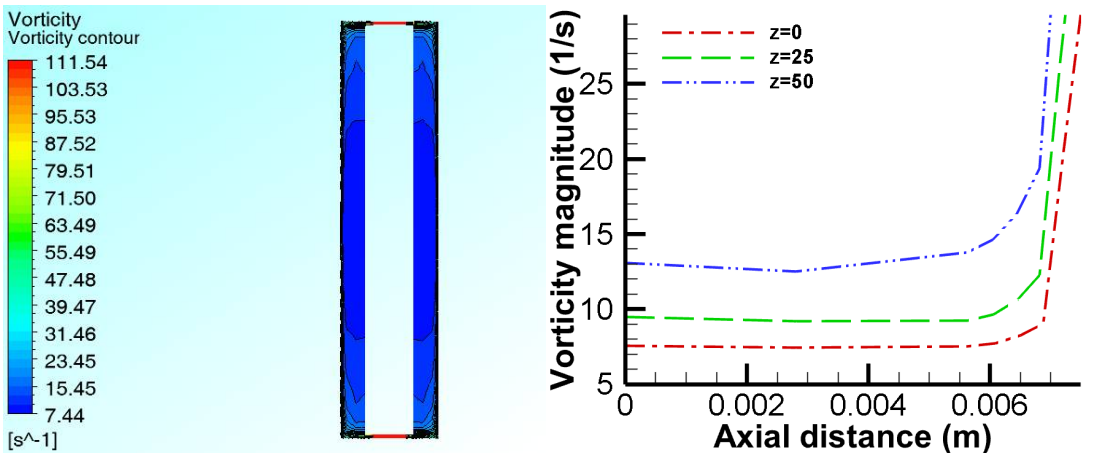

(b)

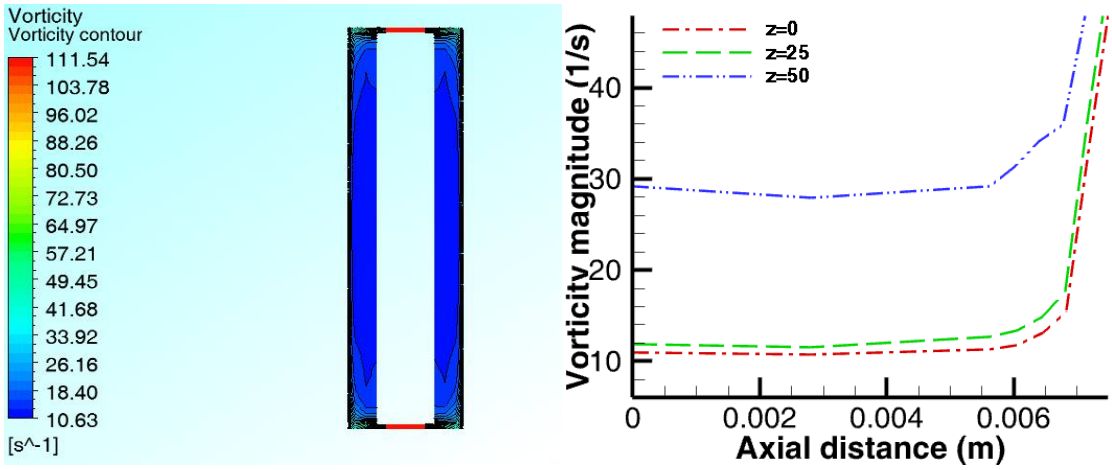

(c)

Fig. 8: Reactor cross sections showing the vorticity amplitude contours and axial vorticity magnitude profiles along three horizontal lines on X-Z plane at *N*=70rpm—RNG model (a) y=0, (b) y=0.025 (c) y=0.045.

4.1.3 Spatial Distribution of Mixing and Turbulence Intensities

The transport phenomena in any engineered system is often controlled by the fluid properties. In the case of stirred tank, the turbulence kinetic energy, intensity or mixing rate of the fluid is the controlling factor [40]. Therefore, in the design of flocculation reactors, it is desirable to have a uniform mixing intensities in the agitation vessel. A quantification of spatial turbulence distribution and mixing efficiency is often carried out on the basis of parameters such as turbulent kinetic energy per unit mass and Reynolds stresses with the Reynolds stress defined as the time-averaged product of velocity signal fluctuations in the fluid flow while the turbulent kinetic energy is the mean kinetic energy per unit mass associated with the turbulent eddies or flow vortex [1,16], It has been suggested that there is a strong correlation between the stirring behaviour in a mixing tank and the turbulence amplitude [16,23]. Flow turbulence within the reactor was investigated at different radial and axial planes to evaluate the mixing efficiency in the reactor. The spatial distribution of the mixing intensities within the reactor expressed as a function of the normal time-averaged Reynolds stresses $\overline{u'u'}$ is shown quantitatively in **Fig. 9a**, while **Fig. 9b** represents the turbulent kinetic energy per unit mass k in terms of the operating speeds at some specific locations in the fluid domain.

In turbulence modelling, the RSM model has been shown to give a more accurate prediction of the turbulence effect especially for flows in which the assumption of isotropic turbulence does not hold such as in swirling and rotating flows involving strong rotation and streamline curvature [31].

Preprints (www.preprints.org) | NOT PEER-REVIEWED | Posted: 29 May 2018 doi:10.20944/preprints201805.0420.v1

Peer-reviewed version available at ChemEngineering 2018, 2, 32; doi:10.3390/chemengineering2030032

The radial distribution of the mixing intensity could be seen to increase with the radius with the highest intensities concentrated on the outer edge of the rotating core while the axial distribution is almost uniform for the lower planes except at y=45 and y=68 where there appears to be variations in the mixing intensity. In terms of the operating speeds, the mixing intensities increases with the radius and the operating speeds as expected in the radial direction. However, there seem to be a region of lower mixing intensities at the reactor wheelspace in the rotating core which means that there is only a marginal improvement in mixing at this location when the operating speed is increased. Overall, the mixing appears to be fairly good except in the region close to the shaft showing somewhat low mixing intensities a small area in the outer region of the rotating core with high mixing intensities. One design modification to improve mixing in the region close to the shaft might be the introduction of baffles on the disc to induce more swirling effect. Similarly, in the outer region with high mixing intensities, the clearance between the disc and the wall can be adjusted to make the mixing more uniform.

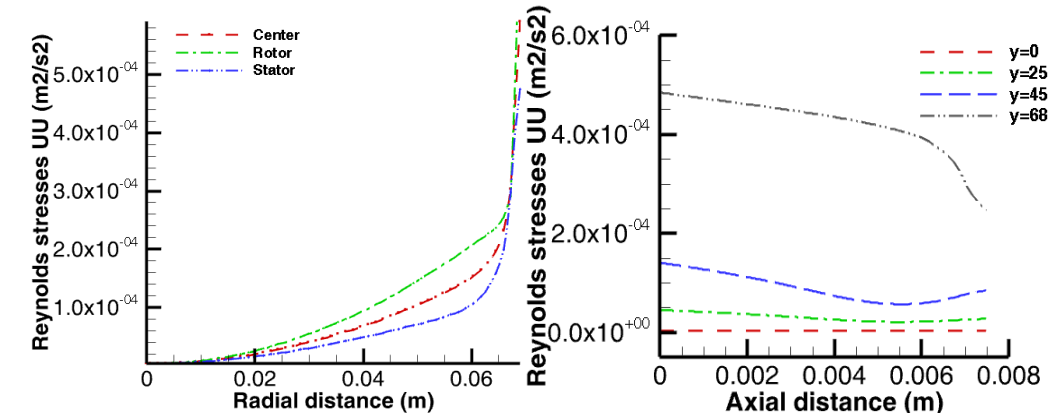

(a)

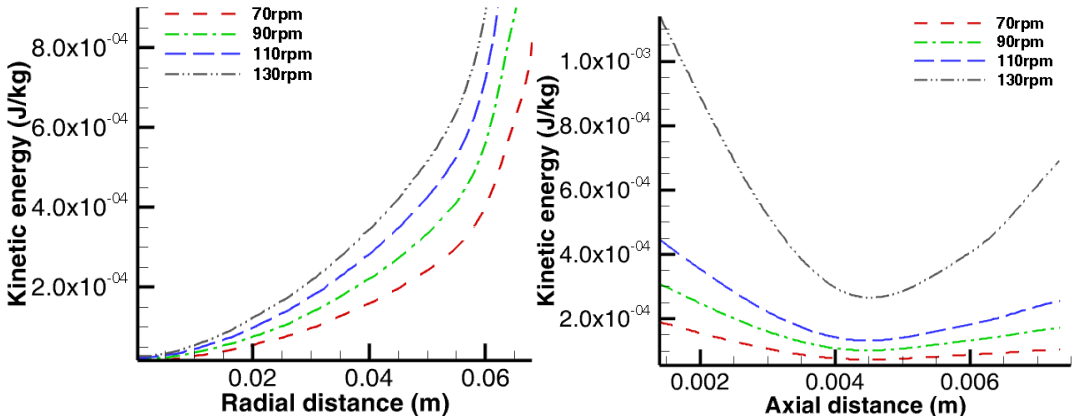

(b)

Fig. 9: Turbulent kinetic energy and Reynolds stresses using RSM model (a) Reynolds stresses' distribution on YZ plane at x=0.0015, 0.003725 and 0.006 and XZ plane parallel to the shaft at y=0, 0.025, 0.045 and 0.068 (b) Turbulent kinetic energy distribution on YZ plane at x=0.003725 and XZ plane parallel to the shaft at y=0.025 for *N*=70-130rpm.

4.1.4 Theoretical Validation of the CFD Model

Fig. 10 shows a comparison of the axial tangential velocity distribution on XZ plane with the Batchelor model predictions. The axial flow streamline in the agglomeration reactor differs somewhat from the Batchelor model and it is assumed that this might be due to differences in the configuration of the rotor-stator systems employed for the studies. The streamlines can be significantly influenced by the vessel geometry and the stirrer configuration thereby resulting in

different gap ratios and flow streamlines. However, **Fig. 10b** shows the presence of separated boundary layers on the rotor and the stator and a rotating core is clearly visible which is consistent with the Batchelor predictions although with minor variation in terms of the extent of the boundary layers. Overall, all the axial tangential velocity profiles (**Fig. 7a-c** and **Fig. 11b**) of the agglomeration reactor confirm the presence of separated boundary layers on the rotor and the stator and an inviscid rotating core.

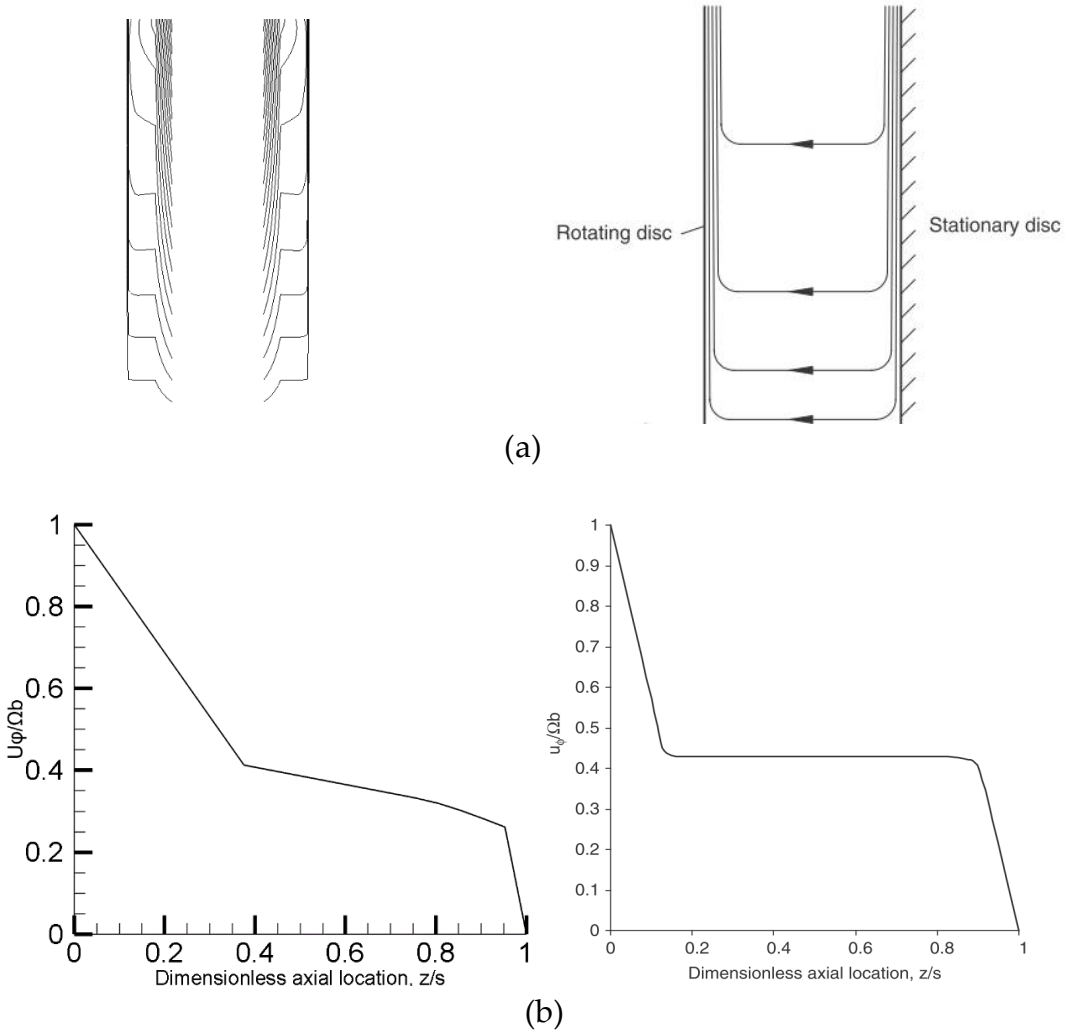

Fig. 11: Flow streamlines for a cross sections of the reactor wheelspace and normalized axial tangential velocity profiles on X-Z plane at *N*=70rpm (a) cross sections of CFD and Batchelor model (b) tangential velocity profile of CFD and Batchelor model at y=0.068 [8].

5. Conclusions

A 3D computational model has been developed to investigate the hydrodynamic characteristics and flow pattern in a rotating disc vortex reactor RVR. A steady state numerical simulation was performed using a single reference frame SRF approach to describe the hydrodynamic interaction between rotating disc and the mixing vessel. A fairly good agreement was obtained between the results of the CFD and the available theoretical and experimental data. A subsequent analysis of the spatial distribution of the hydrodynamic quantities shows that the tangential velocity increases as expected radially across the rotating disc while decreasing in the axial direction with the vorticity magnitude showing only a marginal increase in the radial direction except at the annular space between the disc and the reactor wall, while it increases the axial direction. With respect to the operating speed, the flow parameters' values increase as expected with the operating speed across the fluid domain. The investigation was able to meet the study objectives by identifying regions of

high vorticity—rotation, and poor mixing within the reactor, which are quite useful information in optimizing the reactor performance.

In terms of the fluid flow pattern, the axial velocity distribution across the wheelspace is characterized by laminar Batchelor flow with separated boundary layers and an inviscid core that rotates at a fraction of the rotor angular velocity with an axial pumping effect towards the shroud. The radial tangential velocity profile taken on three planes along the reactor wheelspace however, shows almost a linear distribution with a somewhat lower magnitude between the tip of the disc and the reactor wall while the radial vorticity amplitude is nearly constant except around the tip of the disc. It is anticipated that future studies will address the fluid-particle interactions within the reactor towards a parametric optimization of the wet agglomeration process. A multiphase investigation of the fluid-particle interactions within the reactor will provide an insight into the influence of the hydrodynamics on the temporal and spatial evolution of the specie concentration in the reactor. This information will help in understanding the interplay between the micro-hydrodynamics and the physicochemical processes occurring within the reactor.

6. Patents

The reported rotor-stator RVR agglomeration reactor is a patented device registered with German Patent and Trademark Office, Berlin, Germany with Patent No. DE10 2015 107 682 A1.

Funding: This research was funded by [The World Academy of Sciences TWAS and the National Research Foundation NRF] under the funding instrument number [UID: 105553].

Author Contributions: Conceptualization, B.O. and G.A.; Methodology, B.O. and G.A.; Software, B.O. and M.K.; Validation, B.O. and M.K., Formal Analysis, B.O.; Investigation, Data Curation, B.O. and M.K.; Writing-Original Draft Preparation, B.O.; Writing-Review & Editing, B.O.; Visualization, M.K.; Project Administration, G.A.; Funding Acquisition, B.O. and G.A.

Conflicts of Interest: The authors declare no conflict of interest.

Notations

Re_ϕ	Rotational Reynolds number [-]
ζ	Vorticity magnitude [s^{-1}]
G	Gap ratio [-]
β	Swirl ratio [-]
ρ	Density (kgm^{-3})
δ	Boundary layer thickness [m]
n	Disc rotational speed [s^{-1}]
x	Radial coordinate [m]
z	Axial coordinate [m]
r_d	Rotating disc outer radius [m]
s	Wheelspace or cavity width [m]
μ	Dynamic viscosity [kg $m^{-1}s^{-1}$]
ω	Disc or plate angular velocity [rad s^{-1}]
ω'	Angular velocity of the rotating core [m s^{-1}]
Ω	Disc tangential or tip velocity [m s^{-1}]
U_ϕ	Tangential velocity component [m s^{-1}]
U_r	Radial velocity component [m s^{-1}]
U_z	Axial velocity component [m s^{-1}]
r	Distance along the r-axis [m]
r_s	Shaft radius [m]
r_r	Reactor shroud radius [m]

References

1. Oyegbile, B. *Optimization of Micro Processes in Fine Particle Agglomeration by Pelleting Flocculation*; CRC Press: Leiden, 2016; ISBN 978-1-138-02861-6.

2. Bache, D. H.; Gregory, R. *Flocs in Water Treatment*; IWA Publishing: London, 2007; ISBN 978-1-84339-063-3.

3. Buwa, V.; Dewan, A.; Nassar, A. F.; Durst, F. Fluid Dynamics and Mixing of Single-Phase Flow in a Stirred Vessel with a Grid Disc Impeller: Experimental and Numerical Investigations. *Chem. Eng. Sci.* **2006**, *61*, 2815–2822, doi:10.1016/j.ces.2005.10.066.

4. Dewan, A.; Buwa, V.; Durst, F. Performance Optimizations of Grid Disc Impellers for Mixing of Single-Phase Flows in a Stirred Vessel. *Chem. Eng. Res. Des.* **2006**, *84*, 691–702, doi:10.1205/cherd05044.

5. Utomo, A. T.; Baker, M.; Pacek, A. W. Flow Pattern, Periodicity and Energy Dissipation in a Batch Rotor–Stator Mixer. *Chem. Eng. Res. Des.* **2008**, *86*, 1397–1409, doi:10.1016/j.cherd.2008.07.012.

6. Utomo, A.; Baker, M.; Pacek, A. W. The Effect of Stator Geometry on the Flow Pattern and Energy Dissipation Rate in a Rotor-Stator Mixer. *Chem. Eng. Res. Des.* **2009**, *87*, 533–542, doi:10.1016/j.cherd.2008.12.011.

7. Shevchuk, I. V. *Modelling of Convective Heat and Mass Transfer in Rotating Flows*; Springer: Heidelberg, 2016; ISBN 978-3-319-20960-9.

8. Childs, R. N. P. *Rotating Flow*; Elsevier: Oxford, 2011; ISBN 978-0-12-382098-3.

9. Gan, X. P.; MacGregor, S. A. Experimental Study of the Flow in the Cavity Between Rotating Disks. *Exp. Therm. Fluid Sci.* **1995**, *10*, 379–387, doi:10.1016/0894-1777(94)00099-T.

10. Cheah, S. C.; Iacovides, H.; Jackson, D. C.; Ji, H.; Launder, B. E. Experimental Investigation of Enclosed Rotor-Stator Disk Flows. *Exp. Therm. Fluid Sci.* **1994**, *9*, 445–455, doi:10.1016/0894-1777(94)90022-1.

11. Tu, J.; Yeoh, G. H.; Liu, C. *Computational Fluid Dynamics: A Practical Approach*; 3rd ed.; Butterworth-Heinemann: Oxford, 2018; ISBN 978-0-08-101127-0.

12. Crowe, C. T.; Schwarzkopf, J. D.; Sommerfeld, M.; Tsuji, Y. *Multiphase Flows with Droplets and Particles, Second Edition*; CRC Press: Boca Raton, FL, 2011; ISBN 978-1-4398-4050.

13. Naessens, W.; Maere, T.; Nopens, I. Critical Review of Membrane Bioreactor Models – Part 1: Biokinetic and Filtration Models. *Bioresour. Technol.* **2012**, *122*, 95–106, doi:10.1016/j.biortech.2012.05.070.

14. Naessens W.; Maere, T.; Ratkovich, N.; Vedantam, S.; Nopens, I. Critical Review of Membrane Bioreactor Models – Part 2: Hydrodynamic and Integrated Models. *Bioresour. Technol.* **2012**, *122*, 107–118, doi:10.1016/j.biortech.2012.05.071.

15. Oyegbile, B.; Hoff, M.; Adonadaga, M.; Oyegbile, B. Experimental Analysis of the Hydrodynamics, Flow Pattern and Wet Agglomeration in Rotor-Stator Vortex Separators. *J. Environ. Chem. Eng.* **2017**, *5*, 2115–2127, doi:10.1016/j.jece.2017.04.016.

16. Thomas, S. F.; Rooks, P.; Rudin, F.; Cagney, N.; Balabani, S.; Atkinson, S.; Goddard, P.; Bransgrove, R. M.; Mason, P. T.; Allen, M. J. Swirl Flow Bioreactor Containing Dendritic Copper-Containing Alginate Beads: A Potential Rapid Method for the Eradication of Escherichia Coli from Waste Water Streams. *J. Water Process Eng.* **2015**, *5*, 6–14, doi:10.1016/j.jwpe.2014.10.010.

17. Sievers, M.; Stoll, S. M.; Schroeder, C.; Niedermeiser, M.; Onyeche, T. I. Sludge Dewatering and Aggregate Formation Effects through Taylor Vortex Assisted Flocculation. *Sep. Sci. Technol.* **2008**, *43*, 1595–1609, doi:10.1080/01496390801973888.

18. Wang, X. .; Jin, P. .; Yuan, H. .; Wang, E. .; Tambo, N. Pilot Study of a Fluidized-Pellet-Bed Technique for Simultaneous Solid/liquid Separation and Sludge Thickening in a Sewage Treatment Plant. *Water Sci. Technol.* **2004**, *49*, 81–88.

19. Dionysiou, D. D.; Balasubramanian, G.; (M), M. T. S.; Khodadoust1, A. P.; Baudin, I.; Laîné, J.-M. Rotating Disk Photocatalytic Reactor: Development, Characterization, and Evaluation for the Destruction of Organic Pollutants in Water. *Water Res.* **2000**, *34*, 2927–2940, doi:10.1016/S0043-1354(00)00022-1.

20. Loraine, G.; Chahine, G.; Hsiao, C.-T.; Choi, J.-K.; Aley, P. Disinfection of Gram-Negative and Gram-Positive Bacteria Using DynaJets® Hydrodynamic Cavitating Jets. *Ultrason. Sonochem.* **2012**, *19*, 710–717, doi:10.1016/j.ultsonch.2011.10.011.

21. Kaiser, S. C.; Eibl, R.; Eibl, D. Engineering Characteristics of a Single-use Stirred Bioreactor at Bench-scale The Mobius CellReady 3L Bioreactor as a Case Study. *Eng. Life Sci.* **2011**, *11*, 359–368, doi:10.1002/elsc.201000171.

22. Gao, X.; Kong, B.; Vigil, R. D. Comprehensive Computational Model for Combining Fluid Hydrodynamics, Light Transport and Biomass Growth in a Taylor Vortex Algal Photobioreactor: Lagrangian Approach. *Bioresour. Technol.* **2017**, *224*, 523–530, doi:10.1016/j.biortech.2016.10.080.

23. Escamilla-Ruíz, I. A.; Sierra-Espinosa, F. Z.; García, J. C.; Valera-Medina, A.; Carrillo, F. Experimental Data and Numerical Predictions of a Single-Phase Flow in a Batch Square Stirred Tank Reactor with a Rotating Cylinder Agitator. *Heat Mass Transf.* **2017**, *53*, 2933–2949, doi:10.1007/s00231-017-2030-7.

24. Liu, Z.; Mahdi, R.; Fox, R. O.; Hill, J. C.; Olsen, M. G. Flow Characteristics in a Scaled-up Multi-inlet Vortex Nanoprecipitation Reactor. *Ind. Eng. Chem. Res.* **2015**, *54*, 4512–4525, doi:10.1021/ie5041836.

25. Liu, Z.; Fox, R. O.; Hill, J. C.; Olsen, M. G. A Batchelor Vortex Model for Mean Velocity of Turbulent Swirling Flow in a Macroscale Multi-Inlet Vortex Reactor. *J. Fluids Eng.* **2015**, *137*, 041204-041204–6, doi:10.1115/1.4028784.

26. Oyegbile, B.; Ay, P.; Narra, S. Optimisation of Micro- Processes for Shear Assisted Solid-Liquid Separation in a Rotatory Batch Flow Vortex Reactor. *J. Water Reuse Desalination* **2016**, *6*, 125–136, doi:10.2166/wrd.2015.057.

27. Serra, T.; Colomer, J.; Logan, B. E. Efficiency of Different Shear Devices on Flocculation. *Water Res.* **2008**, *42*, 1113–1121, doi:10.1016/j.watres.2007.08.027.

28. Raffel, M.; Willert, C. E.; Wereley, S. T.; Kompenhans, J. *Particle Image Velocimetry: A Practical Guide*; Springer: Heidelberg, 2007; ISBN 978-3-540-72307-3.

29. Adrian, R. J.; Westerweel, J. *Particle Image Velocimetry*; Cambridge University Press: New York, NY, 2011; ISBN 978-0-521-44008-0.

30. Bridgeman, J.; Jefferson, B.; Parsons, S. A. Computational Fluid Dynamics Modelling of Flocculation in Water Treatment: A Review. *Eng. Appl. Comput. Fluid Mech.* **2009**, *3*, 220–241, doi:10.1080/19942060.2009.11015267.

31. Marshall, E. M.; Bakker, A. Computational Fluid Mixing. In *Handbook of Industrial Mixing: Science and Practice*; Paul, E. L., Atiemo-Obeng, V. A., Kresta, S. M., Eds.; John Wiley & Sons: Hoboken, NJ, 2004; pp. 257–343 ISBN 978-0-471-45145-7.

32. ANSYS, Inc. ANSYS Fluent Theory Guide 18.2 2017.

33. ANSYS, Inc. ANSYS Fluent User's Guide 18.2 2017.

34. Lian, G.; Moore, S.; Heeney, L. Population Balance and Computational Fluid Dynamics Modelling of Ice Crystallisation in a Scraped Surface Freezer. *Chem. Eng. Sci.* **2006**, *61*, 7819–7826, doi:10.1016/j.ces.2006.08.075.

35. Das, S.; Bai, H.; Wu, C.; Kao, J.-H.; Barney, B.; Kidd, M.; Kuettel, M. Improving the Performance of Industrial Clarifiers Using Three-Dimensional Computational Fluid Dynamics. *Eng. Appl. Comput. Fluid Mech.* **2016**, *10*, 130–144, doi:10.1080/19942060.2015.1121518.

36. Schellander, D. *CFD Simulations of Particle Laden Flow: Particle Transport and Separation*; Anchor Academic Publishing: Hamburg, 2014; ISBN 978-3-95489-171-9.

37. Norouzi, H. R.; Zarghami, R.; Sotudeh-Gharebagh, R.; Mostoufi, N. *Coupled CFD-DEM Modeling: Formulation, Implementation and Application to Multiphase Flows*; John Wiley & Sons: Chichester, 2016; ISBN 978-1-119-00513-1.

38. Higashitani, K.; Shibata, T.; Matsuno, Y. Formation of Pellet Flocs from Kaolin Suspension and their Properties. *J. Chem. Eng. Jpn.* **1987**, *20*, 152–157.

39. Walaszek, W.; Ay, P. Pelleting Flocculation—An Alternative Technique to Optimise Sludge Conditioning. *Int. J. Miner. Process.* **2005**, *76*, 173–180, doi:10.1016/j.minpro.2005.01.001.

40. Oyegbile, B.; Ay, P.; Narra, S. Flocculation Kinetics and Hydrodynamic Interactions in Natural and Engineered Flow Systems-A Review. *Environ. Eng. Res.* **2016**, *21*, 1–14, doi:10.4491/eer.2015.086.